Available online at www.sciencedirect.com
SCIENCE DIRECT®
Pergamon
Acta Materialia 51 (2003) 5211–5222
Acta MATERIALIA
www.actamat-journals.com

Stress generation mechanisms in carbon thin films grown by ion-beam deposition

Sulin Zhang [a,*], Harley T. Johnson [b], Gregory J. Wagner [c], Wing Kam Liu [a], K. Jimmy Hsia [d]

[a] *Department of Mechanical Engineering, Northwestern University, 2145 Sheridan Road, Evanston, IL 60208, USA*
[b] *Department of Mechanical and Industrial Engineering, University of Illinois at Urbana-Champaign, Urbana, IL 60801, USA*
[c] *Sandia National Lab, P.O. Box 969, MS 9950, Livermore, CA 94551, USA*
[d] *Department of Theoretical and Applied Mechanics, University of Illinois at Urbana-Champaign, Urbana, IL 60801, USA*

Received 6 May 2003; received in revised form 7 July 2003; accepted 8 July 2003

Abstract

A three-dimensional molecular dynamics (MD) simulation is performed to study the stress generation mechanisms in carbon thin films grown by ion-beam deposition. The relationship between the kinetic energy of incident ions and the steady-state film stress is established. Examination of the atomic stress and film microstructures reveals that the grown films contain a significant fraction of vacancies, contradicting the presumption of the subplantation model. By taking into account both interstitials and vacancies, an analytical model is developed, in which the formation of the compressive stress is attributed to competing mechanisms between generation and recovery of the defects. This model can satisfactorily explain the numerical observation in which compressive stress prevails in films in the presence of vacancies. The present study provides useful insights into tailoring residual stress to control thin film curvature in microelectromechanical systems (MEMS) by ion-beam machining.

Keywords: Carbon thin films; Residual stress; Interstitial; Vacancy

1. Introduction

Diamond-like carbon (DLC) films have found widespread use in the coating industry because of their structural and functional advantages. Interfacial delamination and substrate bending due to the high compressive stress in thin films have become major concerns limiting their performance. Despite extensive studies of the delamination mechanisms and bending in compressively stressed thin films on the micron scale [1,2], the origin of the compressive stress in thin films grown by ion-beam deposition[1] is not well understood and is the focus of the present study.

* Corresponding author. Tel.: +1-847-491-7065; fax: +1-847-491-3915.
E-mail address: s-zhang6@northwestern.edu (S. Zhang).

[1] For the purpose of discussion, all energetic particles whether charged or neutral are referred to here as ions.

1359-6454/$30.00
doi:10.1016/S1359-6454(03)00385-9

When high-energy ions bombard a crystal during the ion-beam deposition, a cascade collision process takes place. On the path of the impact ions, host atoms are displaced from their lattice sites, forming a displacement spike in which defects, such as interstitials and vacancies, are produced. Simultaneously, a significant fraction of the ion kinetic energy is transmitted to the solid in the form of concentrated lattice vibration, forming hot spots—thermal spikes. The thermal energy may activate the migration and recovery of defects. This process leads to a permanent rearrangement of local atoms in the impact area, thus substantially modifying the stress state of the solid.

To date, theoretical models for stress generation due to ion bombardment are highly phenomenological. Within the framework of elasticity, Guinan [3] obtained a rough estimation of thermal stress induced by a single impinging ion in terms of the dissipated energy in the damaged zone. However, it is not straightforward to apply this model to the cases where a number of energetic ions sequentially impact the substrates, since the existing damaged regions may have a strong influence on the subsequent production of defects. Based on the knock-on linear cascade theory, Windischmann [4] predicted a square-root dependence of compressive stress of films prepared by ion-beam sputtering on the incident ion energy. This model, however, is not applicable for sufficiently high ion energy. Davis [5] and Robertson [6] developed a subplantation model in which the compressive stress formation is attributed to the implantation of energetic ions into a subsurface layer of the film. An important implication of this model is that the film is over-dense containing no voids, whereas films are usually under-dense based on experimental measurements and numerical simulations.

A variety of extremely sensitive techniques have been used to monitor the stress evolution in situ in growing films during ion radiations [7–10]. In these experiments, curvature of the films is measured and the stress in a thin film is calculated using Stoney's equation. Volkert [7] performed in situ wafer curvature measurements during amorphization of silicon by MeV ion bombardment. She observed that the compressive stress increases and reaches a peak as amorphous regions are formed. The stress then decreases and reaches a steady-state value as amorphization continues and eventually saturates. Lee et al. [8] used a laser reflection method to monitor the curvature change in DLC films during ion irradiations. They observed that the irradiations result in a decrease in the compressive stress in the DLC films, with final stress state being mildly tensile. Van Dillen et al. [9] measured the stress change in alkali-borosilicate glass samples irradiated by 2 MeV Xe ions. A transition from tensile to compressive stress was observed during the radiation. More recently, ion-beam machining techniques were successfully employed by Bifano et al. [10] to eliminate the curvature of thin films with thickness on the order of several microns in microelectromechanical systems (MEMS). However, the atomic scale mechanisms of stress-state modification in the process of ion-beam machining are not addressed in their study.

On the numeric side, the cascade process by ion irradiation was simulated by Gibson et al. [11]. Using a pair potential, they studied the orbits of the knock-on atoms and the subsequent damage. It was observed from their simulation that the resulting damaged configurations consist of a variety of interstitial–vacancy pairs, that is, Frenkel defects. However, the relationship between the number of Frenkel defects and the knock-on energy was not established due to insufficient sample energies for the impact ions. Molecular dynamics (MD) simulations of stress evolution due to ion flux [12,13] have been limited to the two-dimensional cases. Muller [12] monitored microstructure evolution of Ni films bombarded by Ar neutrals. It was shown that the grown films are under tensile stress. The magnitude of the tensile stress is strongly dependent on the defect concentration and void size distribution in the film, which is in turn determined by the kinetic energy of the impinging particles. Marks et al. [13] studied the relationship between the ion-beam energy and the stress in a growing film on a graphite substrate using MD simulations. A transition from tensile to compressive stress was observed as the kinetic energy of impacting ions changes from 1 to 75 eV. According to their simulation, incident ions insert themselves onto the surface of the growing film rather than penetrate into the substrate, thus contradicting

the subplantation model. Based on this observation, they proposed a new model in which the compressive stress in the grown films is due to a balance between impact-induced compression and thermal spike annealing. However, due to the constraint of the third dimension in their simulation, their MD simulations may not be capable of capturing the realistic dynamics of atomic motion in film growth.

The present study is motivated by the limitations of the theoretical models as well as the discrepancies between theoretical modeling, MD simulations, and experimental observations. In the present work, a three-dimensional MD simulation is performed to simulate deposition of carbon atoms onto an initially perfect (1 1 1) diamond lattice. The residual stress in the growing films is evaluated during the deposition process. A relationship between the steady-state film stress and kinetic energy of incident ions is established. Based on the atomic stress and the structure of grown films from the simulations, an analytical model, which takes into account the competing mechanisms of defect production and recombination, is proposed to interpret stress generation in the deposition process. Results of the MD simulation and the model provide guidelines for reducing the compressive stress in thin films.

The rest of the paper is organized as follows: Section 2 presents MD simulations of growing carbon thin films by an ion-beam deposition process. The stress in the films grown by bombardment of ions with varying kinetic energies is calculated. In Section 3, basic material properties, such as the mass density, the sp^3 fraction, the microstructures and stress distribution of the grown films are examined. Stress generation mechanisms are discussed. Based on the numerical observation, an analytical model is presented in Section 4 to interpret stress generation mechanisms. Discussions and conclusions are presented in Section 5.

2. MD simulations: methods and results

2.1. Film growth

The method of using MD simulations for thin film growth by ion-beam deposition is described elsewhere [14,15], and will therefore be outlined here briefly. The interatomic potential, Φ, between carbon atoms is of Tersoff–Brenner form [16,17]. The total potential of a system containing N atoms, Ψ, is the discrete summation of all the potentials among atoms, as

$$\Psi = \frac{1}{2}\sum_{i}\sum_{j\neq i}\Phi_{ij}(r_{ij}) \tag{1}$$

where index i runs over all the atoms in the system, while index j runs over all the neighbors of atom i within a specified cut-off radius, r_{ij} is the spatial distance between atoms i and j.

The initial substrate is of a perfect diamond lattice consisting of 672 carbon atoms with 56 atoms per layer. Prior to the deposition, the lattice is quasi-statically relaxed to its minimum potential configuration using a conjugate–gradient method. Energetic carbon neutrals are then sequentially deposited onto the substrate with normal incidence and randomly chosen locations. Periodic boundary conditions are applied in the plane perpendicular to the film growth direction. The bottom two layers of the substrate are held fixed. Upon deposition, substrate atoms within a prescribed radius centered at the depositing atom are completely free, while all the other atoms are coupled to an external heat bath employing the method developed by Berendsen et al. [18], as illustrated in Fig. 1. The time constant in the Berendsen method is 125 fs. Based on the actual maximum velocity of the atoms in the system, a varying time-step strategy is introduced to accelerate the simulation. Between two consecutive depositions, the system is thermostated for a relaxation time of approximately 10 ps. Over 900 carbon atoms are deposited to ensure the attainment of a steady-state film growth condition.

2.2. Stress at atomic scale

Within the framework of continuum mechanics, the Cauchy stress at a material point is defined in terms of a resolved force on an area in the limit where the area tends to zero. Such a mechanical definition of stress breaks down at the atomic scale. One of the commonly used definitions of stress for molecular systems is the virial stress. This defi-

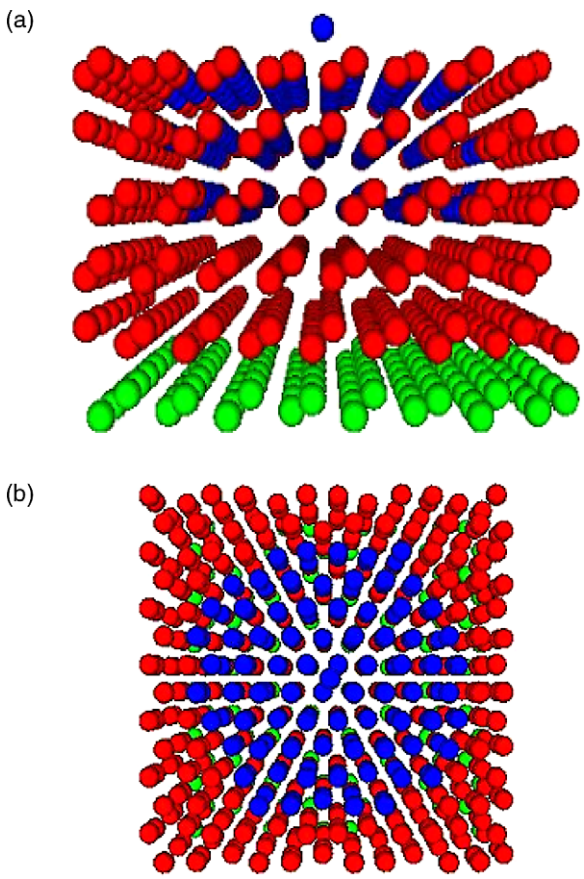

Fig. 1. Initial (1 1 1) diamond lattice as a deposition substrate (red atoms are coupling to an external bath; green atoms are held fixed; blue atoms are completely free). (a) side view, the blue atom on the top of the substrate is the depositing atom; (b) top view.

nition is based on a generalization of the virial theorem of Clausius [19] for gas pressure. In this definition, the average virial stress over an effective volume can be written as a discrete sum of the contribution from all the atoms in the domain of volume Ω:

$$\sigma = \frac{1}{\Omega}\sum_{i}^{N}\left(m_i\dot{\mathbf{r}}_i\otimes\dot{\mathbf{r}}_i + \frac{1}{2}\sum_{j\neq i}\mathbf{r}_{ij}\otimes\mathbf{f}_{ij}\right) \tag{2}$$

where m_i is the mass of atom i, $\dot{\mathbf{r}}_i$ is the time derivative of position $\mathbf{r}_i$, $\mathbf{r}_{ij} = \mathbf{r}_i - \mathbf{r}_j$ is the spatial vector between atoms i and j, and $\otimes$ denotes the tensor product of two vectors. The parameter N is the total number of atoms in the domain. The interatomic force $\mathbf{f}_{ij}$ applied on particle i by particle j is:

$$\mathbf{f}_{ij} = -\frac{\partial\Phi_{ij}\mathbf{r}_{ij}}{\partial r_{ij}\, r_{ij}} \tag{3}$$

The sign convention adopted here for force is positive for repulsion and negative for attraction. Accordingly, a positive stress indicates compression and a negative stress indicates tension.

The stress expression in Eq. (2) includes two parts. The first part stems from the kinetic energy of the atoms, while the second part is from the interatomic forces. For solids, the kinetic energy term is usually small compared to the interatomic force term. Unless otherwise noted, this term is ignored in our calculation.

In continuum mechanics, the volume of the deformed configuration is generally calculated using the deformation gradient and the volume of the undeformed, initial configuration. For the deposition-formed volume, such initial atomic volume is ambiguously defined. An alternative approach is to express the effective volume by $\Omega = N/\rho$, where ρ is the atomic density in the computational domain, and is related to the average bond length, r_{av}, by

$$\frac{\rho}{\rho_{\mathrm{diamond}}} = \left(\frac{r_{\mathrm{diamond}}}{r_{\mathrm{av}}}\right)^3 \tag{4}$$

where ρ_{diamond} is the atom number density per unit volume of a perfect diamond lattice, and r_{diamond} is bond length of a diamond. The relation expressed in Eq. (4) is based on a comparison between an amorphous carbon structure and a perfect diamond lattice.

It should be noted that using Eq. (4) to estimate the volume of an amorphous structure might cause systematic drift since it might not satisfy the sum rule.

2.3. Stress during film growth

Prior to deposition, the substrate is thermostated at 300 K. Due to thermal expansion, a thermal mismatch exists between the bottom two rigid layers and those adjacent to them. Corresponding thermal mismatch stress can be calculated from the thermal

expansion coefficient of a diamond. In calculating the film stress, the thermal stress is ignored since the thermal stress is at least one order of magnitude smaller than the overall stress caused by other effects, as shall be seen later.

Simulations of film growth are performed with seven levels of ion energy: 1, 20, 40, 60, 80, 100 and 150 eV, respectively. It is observed in our simulations that surface sputtering occasionally occurs during depositions. Generally, the higher the incident energy, the more frequent the sputtering. For example, the sputtering rate is approximately 11% of the deposition rate when ion energy is 100 eV, while this number decreases to 6.8% when ion energy is 40 eV. Therefore, the net number of atoms incorporated into the film is less than the number of atoms that are actually deposited. In calculating the film stress, only atoms that fall above the initial free surface of the substrate are considered. The film stress is calculated when the system is fully thermostated after each deposition. Our simulations show that the difference between the in-plane stresses, σ_{xx} and σ_{yy} is very small. In addition, the in-plane normal stresses σ_{xx} and σ_{yy} are at least one order of magnitude larger than the out-of-plane stress and all the shear stresses. Fig. 2(a) shows stress evolution of a film grown with 40 eV ions. In the initial stage of deposition, the biaxial stress exhibits large fluctuations. When over 600 atoms are deposited, the stress gradually approaches a steady-state value of about 5.0 GPa. The film stress is taken to be the linear fit of the steady-state portion of the stress evolution curve. Fig. 2(b) plots the mean biaxial stress, $(\sigma_{xx} + \sigma_{yy})/2$, as a function of kinetic energy of incident ions. It shows that the mean biaxial stress is strongly dependent on the incident energy. The film undergoes tensile stress at low ion energy. A transition from tensile to compressive stress occurs at around 10 eV. The compressive stress peaks when the kinetic energy of the incident ion is around 60 eV. Further increasing the ion energy leads to a gradual decrease in the compressive stress. The overall trend is similar to that predicted by Marks et al. [13], but the magnitude of the compressive stress predicted here is much less than that reported by them. Moreover, the ion energy at which the compressive stress peaks is larger than their prediction. Ion energy larger than 150 eV is not considered in the present simulation due to the increase in the computational cost.

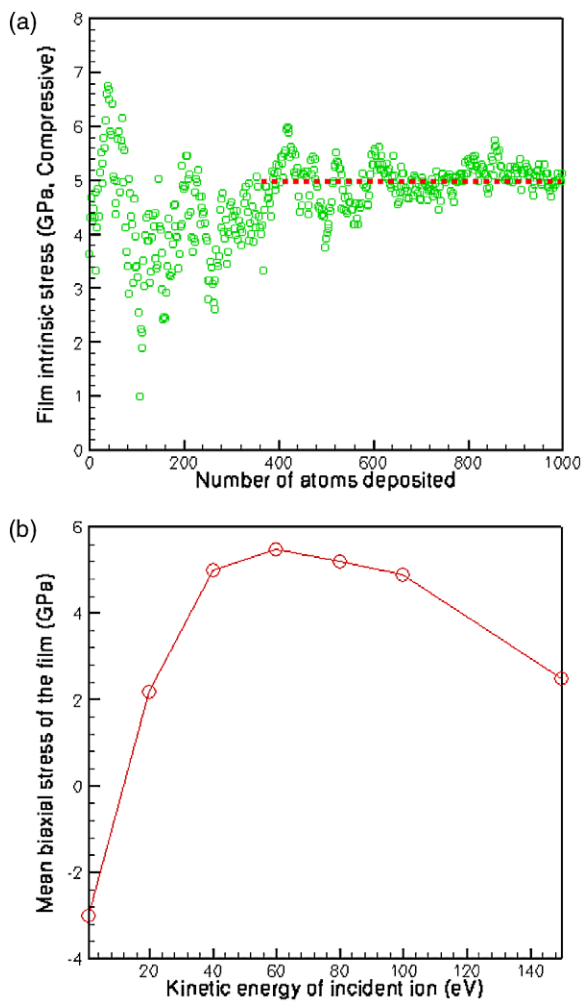

Fig. 2. (a) Compressive stress evolution in a growing film (ion energy = 40 eV); (b) mean biaxial stress versus incident energy (negative value stands for tensile stress, positive value for compressive stress).

3. Stress generation mechanisms

The subplantation model predicts that the compressive stress in the film is caused by ion implantation-induced subsurface densification [5,6]. This model implies that *all* the atoms in the sublayer of

the film undergo compressive stress, and thus is only applicable to over-dense films. Based on a two-dimensional MD simulation, Marks et al. [13] asserted that the compressive stress in thin films is not due to the implantation of energetic ions. They proposed a new model in which the steady-state compressive stress is due to a balance between impact-induced compression and thermal spike annealing.

The two models mentioned above are inconsistent with the observations of our simulation. In testing the validity of these models, basic properties of the grown films are examined. Fig. 3 shows atomic structures of four films grown with 1, 20, 60 and 100 eV ions, respectively. In each film, the red atoms represent those originally in the substrate; the green ones are deposited atoms. All the grown films are amorphous. For 1 eV impact, the substrate atoms and deposited atoms have no interpenetration. For 20 eV impact, the impact ions penetrate into the substrate to a depth of 2–3 layers. Some of the atoms originally in the substrate are mixed with the film atoms. As ion energy increases, the penetration depth and degree of mixing between substrate and film atoms progressively increases. The difference between our numerical observation and that by Marks et al. is obvious: the degree of mixing between substrate atoms and deposited atoms in our simulation is much larger than that in their simulation. Besides using different interatomic potentials, the unrealistic materials and unphysical constraint in the third dimension in their two-dimensional simulation may account for the discrepancy in the results.

Mass densities of the grown films are calculated and shown in Fig. 4. Starting from maximum penetration of the incident ions at which the depth of the film is defined by $d = 0$, the grown films are partitioned into slices with the same thickness in the film growth direction. The original diamond surface is at the depth of $d = 5.3$ Å. The number of atoms in each slice is counted and the mass density for each slice is calculated, and normalized by that of a perfect diamond lattice. From the mass density profile, three regions can be identified: a surface region with the lowest mass density (III); an intrinsic region in which the mass density remains almost constant (II); and a transition region to the substrate (I) [15], as seen in Fig. 4(a). The mass density of the grown films is taken to be the average value over region II. Generally, the relationship of mass density versus incident ion energy follows the same trend as that of stress versus incident ion energy, as seen in Fig. 4(b).

Extensive research over the last decade has been carried out to numerically or experimentally determine the sp^3 fraction in the DLC films, focusing on identifying an optimal deposition condition that promotes sp^3 bonding [15,20–21]. On the one hand, sp^3 bonding is desirable since it makes thin films both mechanically hard and chemically inert. However, a large fraction of sp^3 bonding likely results in high, local compressive stress in the thin films. It is generally accepted that sp^3 fraction directly reflects the damage of the film. The sp^3 bonding is associated with interstitials, while the sp^2 bonding is associated with vacancies. Fig. 5(a) shows the change of number of sp^3-bonded atoms during the growth of film with 60 eV ions. Prior to deposition, there are 560 atoms in the system with sp^3 bonding. The rest of the atoms at the free surface are with sp^2 bonding. At the initial stage of deposition, the sp^3 fraction decreases due to the damage caused by ion implantation. After enough atoms are deposited, the number of sp^3-bonded atoms increases and gradually reaches a steady state, where the number of sp^3-bonded atoms increases linearly with the number of atoms deposited. The sp^3 fraction of the film is taken to be the slope of the linear fit. Fig. 5(b) shows the sp^3 fraction in the film as a function of the ion energy. The results here are consistent with those predicted by previous studies [15,20]. The trend of sp^3 fraction versus ion energy is similar to that of the film stress in Fig. 2(b), indicating an inherent relation between the sp^3 fraction and film stress.

Besides sp^3 fraction, the local atomic stress presents a useful insight into the distribution of the defects in the film. Fig. 6 shows the atomic stress in the film grown with 1 and 60 eV ions, respectively, where the atoms in red undergo local tensile stress, while the atoms in blue undergo local compressive stress. A significant fraction of subsurface atoms undergo tensile stress, indicating that the film contains a large number of vacancies, regardless of the overall stress state. It is well known that,

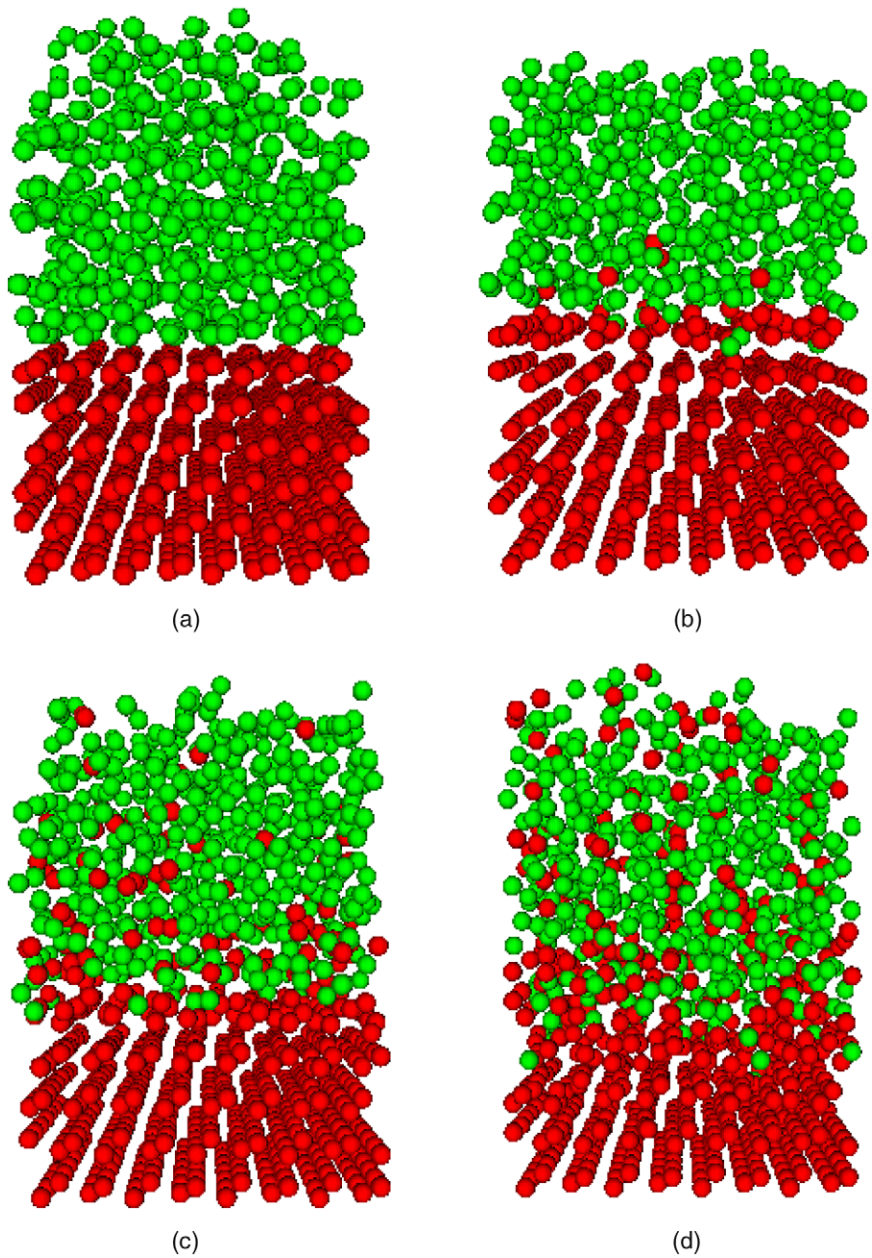

Fig. 3. Atomic structures of grown films (red atoms are originally in substrate, green atoms are deposited ones). (a) 1 eV; (b) 20 eV; (c) 60 eV; (d) 100 eV.

upon energetic particle irradiation, interstitials and vacancies are often formed in pairs in crystals, a defect called Frenkel pairs [22]. It should be mentioned that the amorphous structure and the small sp^3 fraction of the grown films indicates that the films are not crystalline. Thus, the vacancy and the interstitial mentioned here are not defined in the conventional sense. Instead, one can regard a vacancy as a free-volume-excess, and an interstitial as free-volume-shortage in such amorphous structures.

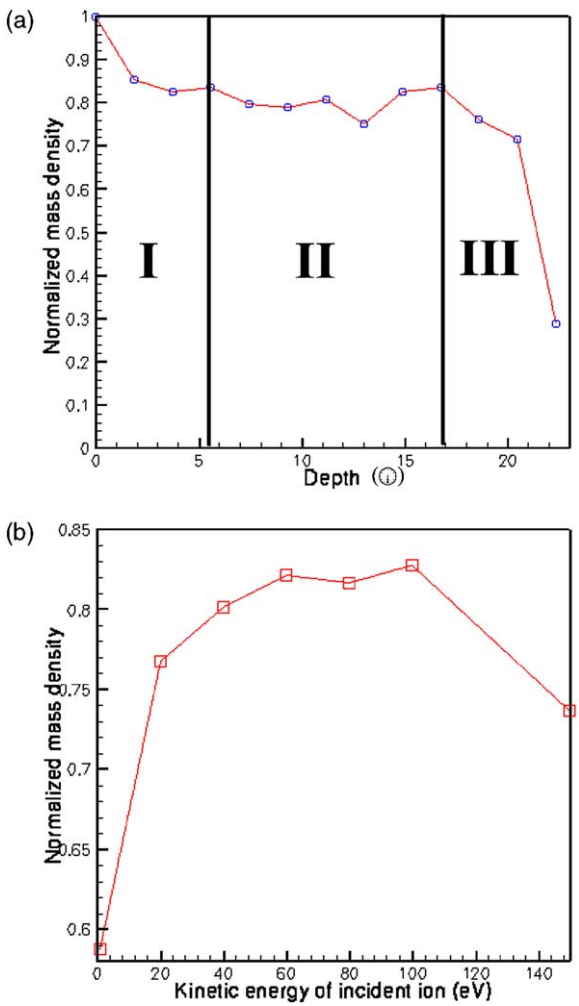

Fig. 4. (a) Depth profile of mass density; (b) mass density versus incident energy.

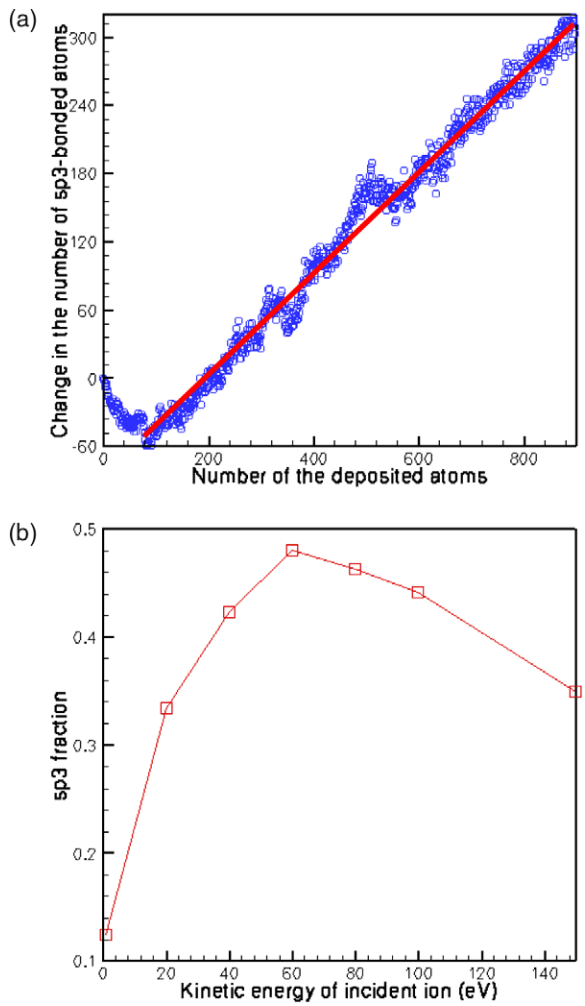

Fig. 5. (a) Change in the number of sp^3-bonded atoms during deposition; (b) sp^3 fraction as a function of ion energy.

4. An analytical model

The above simulation results demonstrate that: (1) penetration occurs when the kinetic energy of incident ions is beyond a critical value; (2) the grown films are under-dense compared with the substrate; and (3) local atomic stress in the grown films is not uniformly in compression. The first observation contradicts with the observation from the two-dimensional simulation, and suggests that the resulting stress may be caused by different mechanisms in different ion energy ranges. The second and third observations indicate that the grown film contains not only interstitials, but also vacancies. The existence of significant fraction of vacancies in the films makes the subplantation model inapplicable. Motivated by these discrepancies between MD simulations and the restriction of the subplantation model, in what follows, we propose a new model to account for the stress generation mechanism.

When striking the substrate, the energetic ions displace atoms from their lattice sites, forming a displacement spike in which defects, such as interstitials and vacancies, are produced. According to the simple model of Kinchin and Pease [23], the

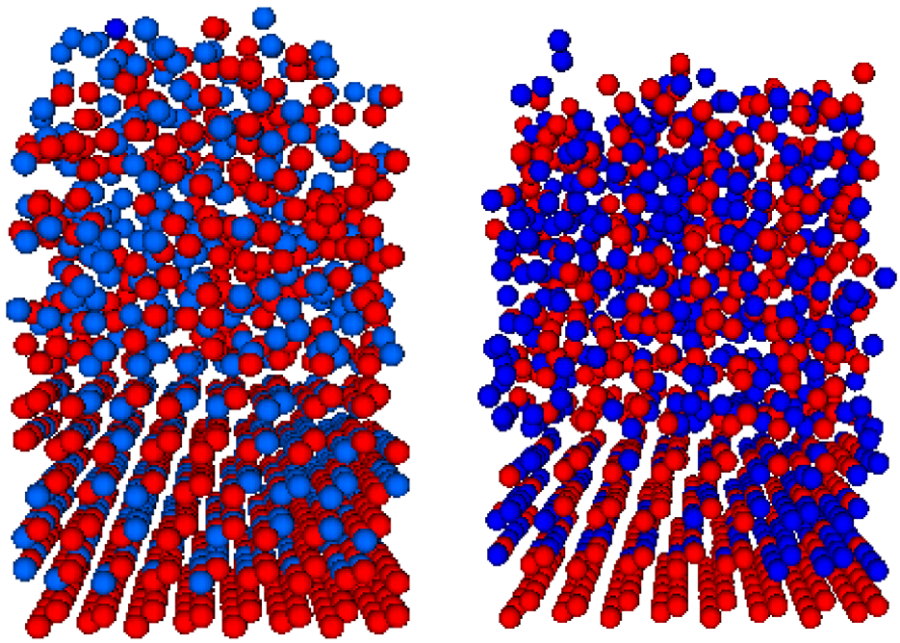

Fig. 6. Atomic stress (red atoms indicate neutral and positive stresses, blue atoms indicate negative stress). (a) 1 eV; (b) 60 eV.

number of displaced atoms produced per ion is given by $N_d = Q/2E_d$, where Q is the kinetic energy of incident ions, E_d is the threshold energy for displacing an atom from its lattice site. The threshold energy depends not only on material properties, but also on the crystallographic direction in which ions impact [23]. The produced defects are *primarily* interstitial–vacancy pairs [11,21]. The rate with which the interstitial–vacancy pairs are created per unit area on the path of ions is related to the number of displaced atoms, N_d. Simultaneously, a significant fraction of the kinetic energy is transferred to concentrated lattice vibration, forming thermal spikes during which members of the defect pairs recombine. The number of recombinations is related to the number of jumps that a defect can make during the lifetime of a thermal spike. According to the calculation done by Seitz and Koehler [24], the number of jumps a defect can make is proportional to $(Q/E_0)^{5/3}$, where E_0 is the activation energy of an interstitial–vacancy pair, and is typically several times less than E_d. The production and recombination of interstitial–vacancy pairs reach a steady state at which the density of defects remains constant. The steady-state density of interstitial–vacancy pairs, ρ_F, can be determined by the following equation:

$$\frac{\rho_F}{\rho_A}\phi_a = \alpha N_d \phi_i - \beta \frac{\rho_F}{\rho_A}\left(\frac{Q}{E_0}\right)^{5/3}\phi_i \tag{5}$$

The left-hand side of Eq. (5) is the net increment rate per unit area of interstitial–defect pairs. It is proportional to the flux of forming atoms, ϕ_a, and the relative density of the defects. The variable ρ_A is the density of the film. The first term on the right-hand side represents the rate per unit area with which defects are produced, which is proportional to the ion flux, $\phi_i(\phi_i > \phi_a)$, and the number of displaced atoms produced per incident ion, N_d. The second term is the rate per unit area with which the defects are recombined, which is proportional to the ion flux, the number of atoms that receive more than the recombination activation energy, and the relative density per unit area of the

defects. The variables α and β are material-dependent coefficients. Solving Eq. (5), one has

$$\frac{\rho_F}{\rho_A} = \frac{\alpha Q/2E_d}{\phi_a/\phi_i + \beta(Q/E_0)^{5/3}} \tag{6}$$

The volumetric strain, ε, is proportional to the density of interstitial–vacancy pairs, and can be written as

$$\varepsilon = \frac{\Delta V}{V} = k\frac{\rho_F}{\rho_A} \tag{7}$$

where k is the ratio of the relaxation volume of an interstitial–vacancy pair and the atomic volume. Within the framework of elasticity, the biaxial stress, σ, in the film is given by

$$\sigma = \frac{Y}{2(1-2\nu)}\varepsilon \tag{8}$$

where Y is the Young's modulus of the film, ν is the Poisson's ratio. Here positive stress represents compression. A simple analysis of Eqs. (6)–(8) shows that the steady-state stress linearly increases at low incident energy ($Q/E_0 \ll (\phi_a/\beta\phi_i)^{3/5}$). The compressive stress reaches a peak at $Q/E_0 = (3\phi_a/2\beta\phi_i)^{3/5}$ with a peak value $\sigma_P = k\frac{Y}{2(1-2\nu)}\frac{\alpha Q/E_d}{5\phi_a/\phi_i}$, beyond which it decreases according to a power-law ($\propto Q^{-2/3}$) for high incident energy. This prediction qualitatively agrees with the results of the MD simulations presented in the previous section. With proper choice of material parameters, the model prediction of the compressive stress as a function of kinetic energy of the incident ions can be calculated using Eqs. (6)–(8), as shown in Fig. 7.

It should be mentioned that the analytical model applies only in the regime where ion penetration occurs (incident ion energy > 10 eV for the present case), and thus cannot be used to account for the tensile stress generated by low energy ions. In addition, the current model considers that the damage of the film is composed of only interstitial–vacancy pairs, and ignores unpaired, isolated interstitials. Nevertheless, an important improvement of our model over the subplanation model is that it can explain the coexistence of compressive stress and vacancies in films.

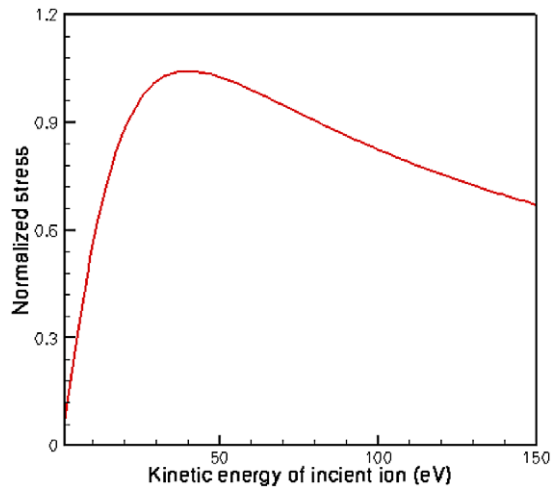

Fig. 7. Compressive stress as a function of kinetic energy of incident ion predicted by Eqs. (6)–(8). Here E_d = 8.0 eV, E_0 = 3.0 eV, α = 1, β = 0.016, ν = 0.2, k = 1, ϕ_a/ϕ_i = 0.8.

5. Concluding remarks

In the present work, MD simulations are performed to investigate the stress generation mechanisms during film growth by ion-beam deposition. The simulations show that the steady-state film stress is found to be strongly dependent on the kinetic energy of the incident ions. Although this finding is consistent with the two-dimensional MD simulations by Marks et al. [13], the deposition dynamics are substantially different. The mixing of the substrate atoms and the newly deposited atoms indicates that energetic ions penetrate below the film surface when the kinetic energy of incident ions is sufficiently high. Detailed examinations of the atomic stress of the grown films provide strong evidence that the film, though in compression, contains not only interstitials, but also a significant fraction of vacancies. This observation contradicts with the presumption of the subplantation model. Based on these analyses, a new model is proposed, where stress generation is attributed to a competing mechanism of generation and recombination of interstitial–vacancy pairs. The theoretical prediction agrees with the MD simulations.

The deposition rate in our simulation is approximately 10 orders of magnitude larger than that in a real experiment in which annealing plays an

important role in determining the final stress state of the films. Within the MD simulation framework described here, it may not be possible to fully account for annealing during such a short elapsed time between ion depositions. In fact, annealing is a thermally activated diffusion processes over a long period of time during which defects heal. MD simulation of such a long-period process would be computationally prohibitive. In the present study, the annealing effect is incorporated into the thermostating process that is mimicked by imposing friction among Langevin atoms. Though artificial, this method accelerates the annealing process, as convinced by the observation of a similar defect-annihilation effect in the present MD simulations. While the simulations are carried out over only very short time scales, they nevertheless demonstrate that a steady state has been reached. The basic mechanisms are believed to be valid over much longer times. These simulation results show that damage due to energetic ions impacting on a surface may be used to modify the residual stress in thin films.

Due to the small time-step and the large number of depositions, the present MD simulation is restricted to a small computational domain. However, the effective range of a displacement and thermal spikes generated by ions with energy less than 200 eV is typically on the order of 1 nm. The size of the computational domain chosen in our simulations ensures that the physical process of interest, defect production and recombination, takes place within the domain. Analysis shows that the compressive stress generation mechanism is relatively insensitive to the size of the computational domain. We conducted a separate simulation with the substrate enlarged by a factor of 1.5 in all the three dimensions, the stress in the film grown at 40 eV agrees with that obtained from the smaller computational domain to within 5%. To more completely address the domain size effect, however, a multi-scale method bridging MD simulations and the continuum scale computations would be necessary.

Besides presenting a mechanism for the formation of compressive stress in the ion-beam deposition process, the results of the present study may have important implications in a novel approach of tailoring thin film shape in MEMS [10], where fine control of the thin film curvature is required. Due to residual stress associated with the micro-fabrication process, free-standing thin films are often curved with the radius of curvature in the range of 10–100 mm. Based on the present study, impacting the concave side of the curved thin film with energetic ions generates compressive stress near the surface of the thin film. According to Bifano et al. [10], this can be used to effectively reduce the curvature of the MEMS thin films. To develop a more precise method of controlling the curvature of such free-standing thin film structures using ion-beam bombardment, work is presently underway to establish relationships between the impact depth, compressive stress and kinetic energy of impact ions.

Acknowledgements

S. Zhang gratefully acknowledges helpful discussions with T. Zhu at MIT; H.T. Johnson acknowledges the support of NSF grant number 0223821; W.K. Liu acknowledges support from NSF and NSF-IGERT; K.J. Hsia acknowledges the partial financial support by NSF grant number CMS 98-72306.

References

[1] Panat R, Zhang S, Hsia KJ. Acta Mater 2003;51:239.
[2] Freund LB, Jonsdottir F. J Mech Phys Solids 1993;41:1245.
[3] Guinan M. Annu Nucl Mater 1974;53:171.
[4] Windischmann H. J Appl Phys 1987;62:1800.
[5] Davis CA. Thin Solid Films 1993;226:30.
[6] Robertson J. Philos Trans R Lond A 1993;342:277.
[7] Volkert CA. J Appl Phys 1991;70:3521.
[8] Lee DH, Fayeulle S, Walter KC, Nastasi M. Nucl Instrum Methods Phys Res B 1999;148:216.
[9] van Dillen T, Brongersma ML, Snoeks E, Polman A. Nucl Instrum Methods Phys Res B 1999;217:221.
[10] Bifano TG, Johnson HT, Bierden P, Mali R. J MEMS 2002;11:592.
[11] Gibson JB, Goland AN, Milgram M, Vineyard GH. Phys Rev 1960;120:1229.
[12] Muller KH. J Appl Phys 1987;62:1796.
[13] Marks NA, McKenzie DR, Pailthorpe BA. Phys Rev B 1996;53:4117.

[14] Liu WK, Karpov EG, Zhang S, Park HS. Comput Methods Appl Mech Engng. 2003. accepted for publication.
[15] Jager HU, Albe KJ. Appl Phys 2000;88:1129.
[16] Tersoff J. Phys Rev Lett 1988;37:6991.
[17] Brenner DW. Phys Rev B 1990;42:95.
[18] Berendsen HJC, Postma JPM, van Gunsteren WF, DiNola A, Haak JR. J Chem Phys 1984;81:3684.
[19] Clausius R. Philos Mag 1870;40:122.
[20] Kaukonen HP, Nieminen RM. Phys Rev Lett 1992;68:620.
[21] Xu S, Flynm D, Tay BK, Prawer S, Nugent KW, Sliva SRP et al. Philos Mag B 1997;76:351.
[22] Wollenberger HJ. In: Cahn RW, Haasen P, editors. Physical metallurgy. 3rd ed. Elsevier Science Publishers BV; 1983. p. 113-9 [Part II, Chapter 17].
[23] Kinchin GH, Pease RS. Rep Prog Phys 1955;18:1.
[24] Seitz F, Koehler JS. Solid State Phys 1956;2:307.